Acta Crystallographica Section A
Foundations of Crystallography
ISSN 0108-7673

Received 27 August 2002
Accepted 6 January 2003

Theory of diffraction from $D0_{19}$ ordered c.p.h. structures containing complex stacking faults on basal planes

P. Ghosal† and S. Lele*

Centre of Advanced Study, Department of Metallurgical Engineering, Institute of Technology, Banaras Hindu University, Varanasi-221005, India. Correspondence e-mail: slele@satyam.net.in

Antiphase boundaries and stacking faults affect the deformation behaviour of intermetallics. In an ordered c.p.h. (close-packed hexagonal) structure of $D0_{19}$ type (*e.g.* Mg_3Cd, Ti_3Al-based alloys), stable planar faults of two types are possible on the basal plane. These are antiphase boundaries (APBs) and complex stacking faults (CSFs), which are a combination of an APB and a stacking fault. The latter can be either of shear or of climb type. If the bounding partial dislocations of a CSF lie in its plane, then it is designated as a shear CSF, otherwise it is called a climb CSF. A mathematical formulation of the theory of diffraction from a $D0_{19}$ structure having a shear or climb type of CSF has been carried out. The diffraction effects owing to the presence of these CSFs have been found. Integrated intensities and widths of the reflections are affected. These have been evaluated in terms of the probability of the occurrence of these faults.

1. Introduction

Antiphase boundaries (APBs) significantly affect the deformation behaviour of intermetallics. Various types of APB are possible in the ordered close-packed hexagonal (c.p.h.) $D0_{19}$ structure depending on the shift vector and the planes to which these planar faults are parallel (Ghosal *et al.*, 1993). Complex stacking faults (CSFs) are characterized by a combination of an APB and a stacking fault (SF) on the basal plane. These planar faults can be formed during the passage of dislocations through an ordered crystal or during growth and impingement of different nuclei of order. The former will lead to the formation of shear CSFs while the latter will give rise to climb CSFs.

The first mathematical formulation of the theory of X-ray diffraction from APBs was carried out by Wilson (1943) (see also Wilson & Zsoldos, 1966) for the $L1_2$ structure (ordered face-centred cubic, Cu_3Au type). Extensive X-ray studies on Cu_3Au have been undertaken by Mikkola & Cohen (1965, 1966). Studies of diffraction from APBs and CSFs in another important structure, namely the ordered c.p.h. $D0_{19}$ type, exhibited notably by Mg_3Cd and Ti_3Al, seem to be limited. Prasad (1975) has worked on the theory of diffraction from CSFs and APBs on basal planes in the $D0_{19}$ structure. He has considered shear CSFs (denoted SF + APB by him) arising from different crystallographically equivalent shift vectors to be independent of each other. We believe that this distinction is not physically realistic. The detailed differences between our approach and that of Prasad are discussed later. Further, he has not considered climb CSFs. We formulate here the theory of diffraction from shear and climb CSFs. These CSFs affect the reflections in two ways, namely by changing the integrated intensity and by broadening the reflections. It needs to be mentioned that, in the absence of ordering, shear and climb CSFs on the basal plane will reduce to deformation and growth faults, respectively. Wilson (1942) pioneered the formulation of the theory of diffraction from growth faults in c.p.h. structures while Christian (1954) considered deformation faults subsequently. The formulation of the theory is subject to the following assumptions usual in this type of work: (i) the crystal is infinite in size and free of distortions; (ii) there is no change in the lattice spacing at the CSFs; (iii) the CSFs are distributed at random; and (iv) the CSFs extend over entire domains.

2. Geometrical structure of shear CSFs

Consider the $D0_{19}$ structure shown in Fig. 1. Fig. 2 gives its basal plane projection. Atoms on *A*, *B* and *C* layers are represented respectively by large, medium and small circles. Atomic species *A* and *B* are represented respectively by open and filled circles. The sublattices I, II, III and IV are marked in one unit cell. Here, the sites in the *A* layer are at zero height while those in the *B* layer are at a height of $\frac{1}{2}c$, which is shown by $\frac{1}{2}$ in one part of the figure. All sites in the *A* layer are joined by continuous lines. *B* atoms occupy sublattice type IV sites while *A* atoms occupy sublattice sites of types I, II or III as shown in one unit cell. The letters *A* and *B* refer to the type of

† Present address: Defence Metallurgical Research Laboratory, Kanchanbagh, Hyderabad 500 058, India. E-mail: parthaghosal@yahoo.co.in.

close-packed layers as well as the type of atoms. However, this should not cause any confusion, as the context will clarify the meaning. Important directions are shown in the usual Miller–Bravais notation while the corresponding planes are perpendicular to the respective directions in this particular case.

A shear CSF can be created by a virtual process in which one part of the crystal is shifted relative to the other part by a vector denoted as the shift vector. We will consider here shift vectors parallel to the basal plane that give rise to a shear or mechanical type of CSF. The initial sequence of layers can be written as

$$\ldots A^{\rm IV}B^{\rm IV}A^{\rm IV}B^{\rm IV}\ldots,$$

where A and B indicate the layer type and the superscript indicates the sublattice type occupied by B atoms. We now consider the effect of the shift vector $(1/6)[1\bar{1}00]$. This moves atoms lying initially at A positions to C positions (see Fig. 2). Further, the B atoms now occupy sites of sublattice I instead of IV. The first change corresponds to the creation of an intrinsic or deformation stacking fault while the second change leads to the simultaneous formation of an APB. Thus, this fault is a CSF. We can write the layer sequence as follows:

$$\ldots A^{\rm IV}B^{\rm IV}\,\vdots\,C^{\rm I}A^{\rm I}\ldots,$$

where the vertical dotted line indicates the position of the CSF. Such a fault can also occur after an $A^{\rm IV}$ layer instead of $B^{\rm IV}$. In this case, the shift vector becomes $(1/6)[\bar{1}100]$, which is equal in magnitude and opposite in direction to the earlier shift vector. The layer sequence in this case is given by

$$\ldots B^{\rm IV}A^{\rm IV}\,\vdots\,C^{\rm I}B^{\rm I}\ldots.$$

The shift vectors $(1/6)[\bar{1}010]$ and $(1/6)[01\bar{1}0]$ lead to shear CSFs after $B^{\rm IV}$ layers, owing to which B-atom occupancy changes to sublattice types II and III, respectively. CSFs occurring after $A^{\rm IV}$ layers have opposite shift vectors.

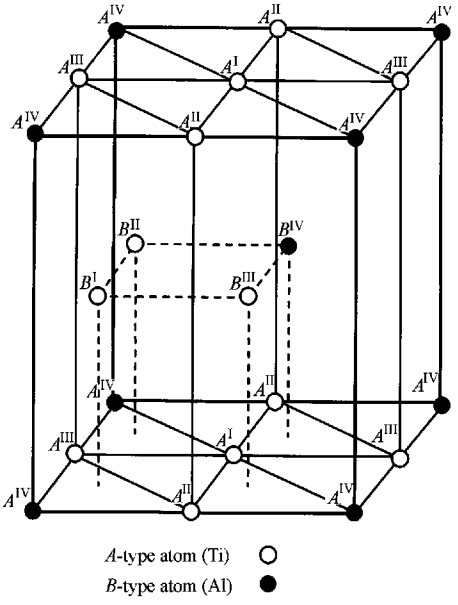

Figure 1
$D0_{19}$ ordered c.p.h. structure. Empty circles denote A atoms and filled circles denote B atoms of an A_3B alloy.

3. Geometrical structure of climb CSFs

A climb CSF can arise through the following virtual process. Begin by considering a normal sequence of layers as shown below:

$$\ldots A^{\rm IV}B^{\rm IV}A^{\rm IV}B^{\rm IV}A^{\rm IV}B^{\rm IV}\ldots.$$

First remove one layer (say $A^{\rm IV}$ indicated by adjoining vertical lines in the first sequence below). In the new sequence, a $B^{\rm IV}$ layer is followed by another $B^{\rm IV}$ layer. This sequence is very unfavourable energetically and the system can lower its energy by a shift of the right half of the crystal (to the right of the vertical line in the second sequence below) by $(1/6)[\bar{1}100]$ changing the $B^{\rm IV}$ layer to a $C^{\rm I}$ layer. The position of the succeeding $A^{\rm IV}$ layer shifts to that of a $B^{\rm I}$ layer as shown in the last sequence below.

$$\begin{aligned}
&\ldots A^{\rm IV}B^{\rm IV}\,|\,A^{\rm IV}\,|\,B^{\rm IV}A^{\rm IV}\ldots && (1/2)[000\bar{1}]\\
&\ldots A^{\rm IV}B^{\rm IV}\,|\,B^{\rm IV}A^{\rm IV}\ldots && +(1/6)[\bar{1}100]\\
&\ldots A^{\rm IV}B^{\rm IV}\,|\,C^{\rm I}A^{\rm I}\ldots && =(1/6)[\bar{1}10\bar{3}].
\end{aligned}$$

As is clear from the final sequence of layers, the virtual process described above leads to the formation of a composite fault made up of a growth fault and an APB. Since the shift vector, $(1/6)[\bar{1}10\bar{3}]$, is not parallel to the basal plane, we can call this a climb CSF.

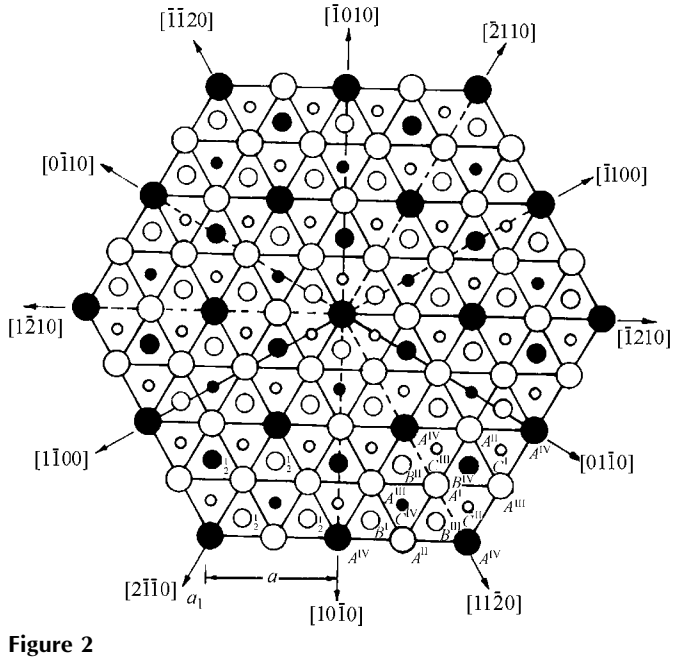

Figure 2
Basal plane projection of $D0_{19}$ structure. Atoms on A, B and C layers are represented respectively by large, medium and small circles. Atomic species A and B are represented respectively by open and filled circles. The sublattices I, II, III and IV are marked in one unit cell.

4. General expression for the diffracted intensity

In terms of the conventional hexagonal basis vectors $\mathbf{a}_1$, $\mathbf{a}_2$, $\mathbf{a}_3$ ($\mathbf{a}_1$ and $\mathbf{a}_2$ being double the lattice vectors of the disordered c.p.h. structure and $\mathbf{a}_3$ being equal to that for the disordered structure), the position vector $\mathbf{R}_m$ of a unit cell at the (m_1m_2) position in layer m_3 of a possibly faulted $D0_{19}$ crystal is given by

$$\mathbf{R}_m = m_1\mathbf{a}_1 + m_2\mathbf{a}_2 + \tfrac{1}{2}m_3\mathbf{a}_3 + \mathbf{Q}_{m_3}, \quad (1)$$

where $\mathbf{Q}_{m_3}$ is the displacement vector in the plane of the layer. This vector takes different values in the presence or absence of a CSF.

The diffracted intensity from such a crystal is given by (Warren, 1969)

$$\begin{aligned} I(h_3) &= N\psi^2 \sum_m \langle \exp[i\phi_m]\rangle \exp[\pi i m h_3] \\ &= N\psi^2 \sum_m J_m \exp[\pi i m h_3], \end{aligned} \quad (2)$$

where N is the number of layers and ψ^2 is the intensity scattered by one layer. The phase difference ϕ_m between rays diffracted from the mth layer and the layer at the origin is given by

$$\phi_m = 2\pi(h\mathbf{b}_1 + k\mathbf{b}_2 + h_3\mathbf{b}_3)\cdot\mathbf{Q}_m, \quad (3)$$

where $\mathbf{b}_1$, $\mathbf{b}_2$, $\mathbf{b}_3$ are reciprocal-lattice vectors and hkh_3 are the corresponding coordinates of the reciprocal-lattice point with h and k being integers and h_3 a continuous variable.

It is evident that the problem of determining the diffracted intensity reduces to finding the values of J_m. To evaluate J_m, we express the phase difference as the sum of two phase differences and then replace the average of this sum by the product of their averages. Thus,

$$\begin{aligned} \langle \exp[i\phi_m]\rangle &= \langle \exp[i\phi_{m-1}] \exp[i(\phi_m - \phi_{m-1})]\rangle \\ &= \langle \exp[i\phi_{m-1}]t\rangle \langle \exp[i(\phi_m - \phi_{m-1})]\rangle. \end{aligned} \quad (4)$$

Denoting $(\phi_m - \phi_{m-1})$ by $\delta\phi_{m,m-1}$ and the corresponding probability of the occurrence of such a phase difference by $P_{m,m-1}$, we have

$$\langle \exp[i\phi_m]\rangle = \sum \langle \exp[i\phi_{m-1}]\rangle P_{m,m-1} \exp[i\delta\phi_{m,m-1}], \quad (5)$$

where the summation extends over all possible values of $\delta\phi_{m,m-1}$. This leads to a recurrence relation, which can be solved by using initial conditions (Prasad & Lele, 1971). Values of $P_{m,m-1}$ for all possible values of $\delta\phi_{m,m-1}$ are depicted in a probability tree as discussed below.

5. Diffraction theory for shear CSFs on basal planes

To construct the probability trees, we adopt the following procedure. Consider an A-type layer with B atoms on site IV to be present on the $(m-1)$ layer. In the absence of a shear CSF, the next layer will be a B-type layer with B atoms again on site IV. Similarly, an A^{IV} layer will follow a B^{IV} layer in the absence of a shear CSF. The displacements and corresponding phase differences in the two cases will respectively be

$$(1/3)[1\bar{1}00] = (1/3)[1\bar{1}0]; \quad (2\pi/3)(h-k)$$

and

$$(1/3)[\bar{1}100] = (1/3)[\bar{1}10]; \quad (2\pi/3)(-h+k).$$

In the presence of shear CSFs, the layer type, namely A, B or C, can change. However, if there is no shear CSF between a pair of layers, the phase difference between these layers is not altered owing to the presence of shear CSFs at any other location. To account for this fact, we will give a subscript 0 or 1 to the layer type (for example A_0^{IV} or A_1^{IV}), depending on the phase difference to the next layer (B_1^{IV} or C_0^{IV}) being $(2\pi/3)(h-k)$ or $(2\pi/3)(-h+k)$, respectively, in the absence of a shear CSF.

As mentioned earlier, in the presence of a shear CSF an A_0^{IV} layer, say, will be followed by a C_1^{I} layer. The displacement vector for this case can be found by adding the displacement vector without a shear CSF and the component of the shift vector parallel to the plane of the CSF and is given by

$$(1/3)[1\bar{1}00] + (1/6)[\bar{1}100] = (1/6)[1\bar{1}00] \equiv (1/6)[1\bar{1}0].$$

Thus, the phase difference will be $(2\pi/6)(h-k)$. It can be shown by consideration of Fig. 2 that the same phase difference occurs for the following transitions in the presence of a shear CSF:

(1) $B_0^{IV} \rightarrow A_1^{I}$, (2) $C_0^{IV} \rightarrow B_1^{I}$, (3) $A_0^{I} \rightarrow C_1^{IV}$, (4) $B_0^{I} \rightarrow A_1^{IV}$, (5) $C_0^{I} \rightarrow B_1^{IV}$, (6) $A_0^{II} \rightarrow C_1^{III}$, (7) $B_0^{II} \rightarrow A_1^{III}$, (8) $C_0^{II} \rightarrow B_1^{III}$, (9) $A_0^{III} \rightarrow C_1^{II}$, (10) $B_0^{III} \rightarrow C_1^{II}$, (11) $C_0^{III} \rightarrow B_1^{II}$.

In the same way, the displacement vectors and the phase differences can be found for shear CSFs with the other two possible shift vectors (Ghosal, 1996). In each case, we denote the probability of occurrence of a shear CSF by α and thus the probability for absence of a shear CSF is $(1-3\alpha)$.

Taking the above facts into account, a probability tree has been constructed and is shown in Fig. 3 along with the phase differences. Similar trees can be drawn starting from B_0 or C_0 layers by cyclic permutation. This figure also shows the possibilities for transition from an $(m-2)$ layer of type B_1^{IV}. Using these trees, as well as similar ones, one can construct a slightly different type of tree which shows all possible ways of reaching a particular type of layer. Two typical trees of this type are shown in Fig. 4.

We can write difference equations for J_m using the trees constructed above. We distinguish the values of J_m for stacking sequences terminating with layers having subscript 0 (say A_0^{IV}) or 1 (say B_1^{IV}) by giving the same superscript.

$$J^1_{m+1} = \left\{(1-3\alpha)\exp\left[\frac{2\pi i}{3}(-h+k)\right] + \alpha\exp\left[\frac{2\pi i}{6}(2h+k)\right] + \alpha\exp\left[\frac{2\pi i}{6}(-h+k)\right] + \alpha\exp\left[\frac{2\pi i}{6}(-h-2k)\right]\right\}J^0_m \quad (6)$$

$$J^0_m = \left\{(1-3\alpha)\exp\left[\frac{2\pi i}{3}(h-k)\right] + \alpha\exp\left[\frac{2\pi i}{6}(-2h-k)\right] + \alpha\exp\left[\frac{2\pi i}{6}(h-k)\right] + \alpha\exp\left[\frac{2\pi i}{6}(h+2k)\right]\right\}J^1_{m-1}. \quad (7)$$

Introducing the following abbreviations for convenience,

$$\varepsilon = \exp[(2\pi i/6)(h-k)], \quad \eta = 1 + (-1)^h + (-1)^k, \quad (8)$$

we have

$$J^1_{m+1} = [(1-3\alpha)\varepsilon^2 + \alpha\varepsilon\eta]J^0_m \quad (9)$$

$$J^0_m = [(1-3\alpha)\varepsilon^{*2} + \alpha\varepsilon^*\eta]J^1_{m-1}, \quad (10)$$

where * denotes complex conjugation. Substituting from (10) into (9) and simplifying, we obtain

$$J^1_{m+1} = [(1-3\alpha)^2 + 2\alpha(1-3\alpha)\eta\cos(2\pi/6)(h-k) + \alpha^2\eta^2]J^1_{m-1} \quad (11)$$

This is the so-called characteristic equation and has solutions of the form

$$J_m = C\rho^m. \quad (12)$$

Thus, (11) becomes

$$\rho^2 = (1-3\alpha)^2 + 2\alpha(1-3\alpha)\eta\cos(2\pi/6)(h-k) + \alpha^2\eta^2 = (\pm Z)^2. \quad (13)$$

This quadratic equation has two solutions: Z_0 and $-Z_1$ with $Z_0 = Z_1 = Z$. Consideration of different possible values of h and k shows that the values of Z reduce to the following:

(a) h and k even (fundamental reflections):

(i) $h - k = 3N$:

$$Z = 1. \quad (14)$$

(ii) $h - k = 3N \pm 1$:

$$Z = (1 - 9\alpha + 27\alpha^2)^{1/2}. \quad (15)$$

(b) h or k odd (superlattice reflections):

(i) $h - k = 3N$:

$$Z = (1 - 4\alpha). \quad (16)$$

(ii) $h - k = 3N \pm 1$:

$$Z = (1 - 5\alpha + 7\alpha^2)^{1/2}. \quad (17)$$

Fundamental reflections with $h - k = 3N$ are unaffected (since Z is independent of α) while those with $h - k = 3N \pm 1$ show a dependence on α. All superlattice reflections show a dependence on α which is different for different $(h - k)$ values.

Corresponding to the two roots of ρ, namely $+Z_0$ and $-Z_1$, we can write a general solution for (12) of the form

$$J_m = C_0(Z_0)^m + C_1(-Z_1)^m, \quad m \geq 0. \quad (18)$$

A little consideration shows that, for negative values of m, we can write

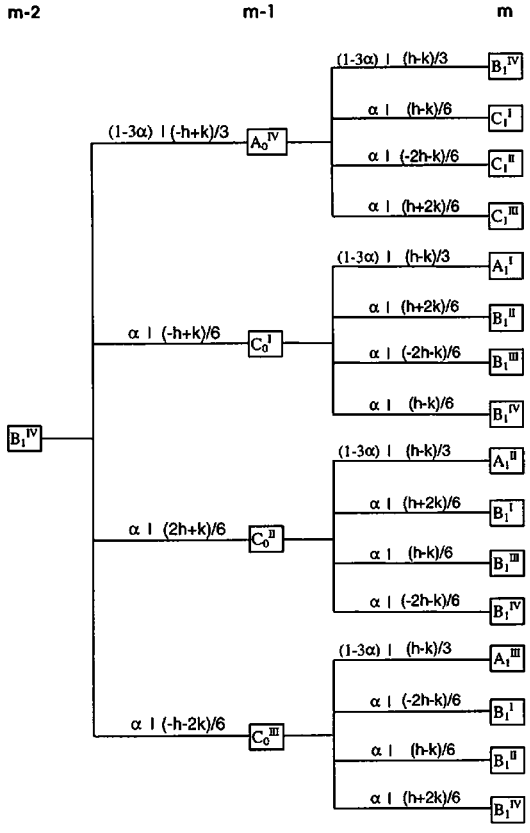

Figure 3
Probability tree showing the probability of occurrence of shear CSFs. The corresponding phase differences in units of 2π are also indicated.

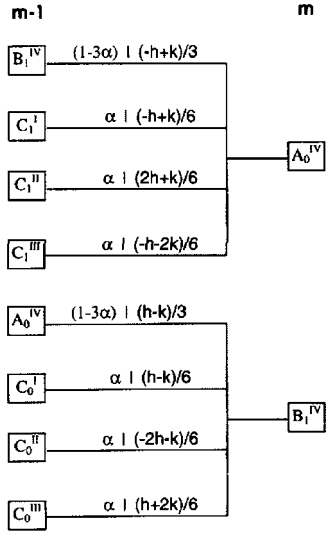

Figure 4
Probability trees showing all possible ways of reaching a particular type of layer in the presence of shear CSFs.

$$J_m = C_0(Z_0)^{|m|} + C_1(-Z_1)^{|m|}, \quad m < 0. \tag{19}$$

Here, C_0 and C_1 are to be evaluated from the initial conditions *i.e.* values of J_m for $m = 0$ and 1. These can be found by direct computation from the probability trees.

$$J_0 = 1 \tag{20}$$

and

$$J_1 = \tfrac{1}{2}[(1-3\alpha)\varepsilon^2 + \alpha\varepsilon\eta + (1-3\alpha)\varepsilon^{*2} + \alpha\varepsilon^*\eta]. \tag{21}$$

Substituting the values found above for J_0, J_1 and Z in (18), we obtain C_0 and C_1 for different values of h and k.

(*a*) h and k even (fundamental reflections):

(i) $h - k = 3N$:

$$C_0 = 1; \quad C_1 = 0. \tag{22}$$

(ii) $h - k = 3N \pm 1$:

$$C_0 = \tfrac{1}{2} - \frac{1}{4(1-9\alpha+27\alpha^2)^{1/2}}$$
$$C_1 = \tfrac{1}{2} + \frac{1}{4(1-9\alpha+27\alpha^2)^{1/2}}. \tag{23}$$

(*b*) h or k odd (superlattice reflections):

(i) $h - k = 3N$:

$$C_0 = 1; \quad C_1 = 0. \tag{24}$$

(ii) $h - k = 3N \pm 1$:

$$C_0 = \tfrac{1}{2} - \frac{(1-4\alpha)}{4(1-5\alpha+7\alpha^2)^{1/2}}$$
$$C_1 = \tfrac{1}{2} + \frac{(1-4\alpha)}{4(1-5\alpha+7\alpha^2)^{1/2}}. \tag{25}$$

6. Diffraction theory for climb CSFs on basal planes

As discussed earlier, in the presence of climb CSFs, the layer type A, B or C can change. Further, even if there is no climb CSF between a successive pair of layers, the phase difference between these layers may be altered owing to the presence of climb CSFs at other locations. This is due to the removal of a layer at a climb CSF. However, as in the case of shear CSFs, subscripts 0 or 1 can be assigned to the layers to account for this change, depending on the displacement to the next layer in the absence of a climb CSF being $+(1/3)[1\bar{1}00]$ or $-(1/3)[1\bar{1}00]$, respectively. With this assignment, the stacking sequences in the absence and presence of climb CSFs become:

$$\begin{matrix} \ldots A_0^{\rm IV} B_1^{\rm IV} \;\; A_0^{\rm IV} B_1^{\rm IV} \ldots \\ \ldots A_0^{\rm IV} B_1^{\rm IV} \vdots C_1^{\rm I} B_0^{\rm I} \ldots \end{matrix} \quad (1/6)[\bar{1}10\bar{3}].$$

In this sequence, the subscript 1 repeats at a climb CSF unlike in the normal sequence. Similarly, we can produce a climb CSF after an $A_0^{\rm IV}$ layer by the following steps:

$$\ldots B_1^{\rm IV} A_0^{\rm IV} \vdots B_1^{\rm IV} \vdots A_0^{\rm IV} B_1^{\rm IV} \ldots \quad (1/2)[000\bar{1}]$$
$$\ldots B_1^{\rm IV} A_0^{\rm IV} \vdots A_0^{\rm IV} \;\; B_1^{\rm IV} \ldots \quad + (1/6)[1\bar{1}00]$$
$$\ldots B_1^{\rm IV} A_0^{\rm IV} \vdots C_0^{\rm I} \;\; A_1^{\rm I} \ldots \quad = (1/6)[1\bar{1}0\bar{3}].$$

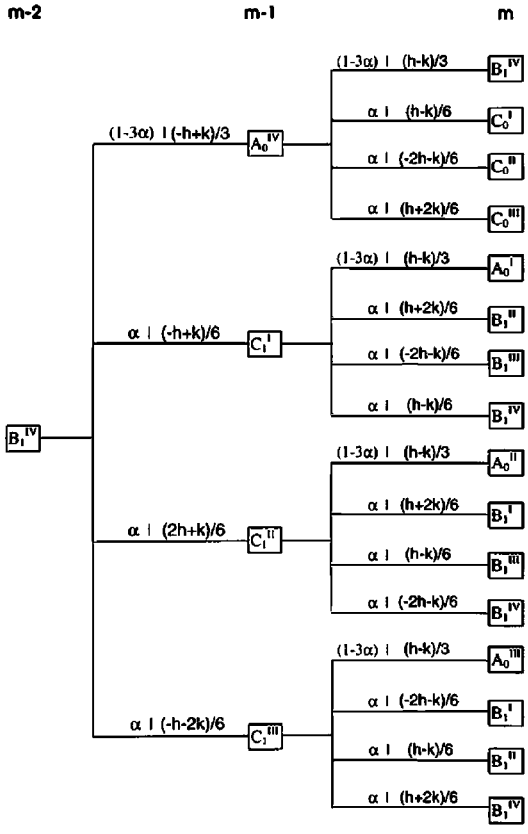

Figure 5
Probability tree showing the probability of occurrence of climb CSFs along with the corresponding phase differences.

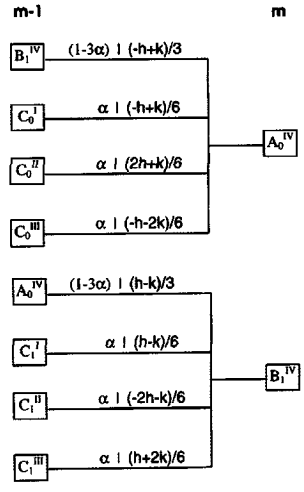

Figure 6
Probability trees showing all possible ways of reaching a particular type of layer in the presence of climb CSFs.

The displacement vector for this case can be found by adding the displacement vector without a CSF and the component of the shift vector parallel to the plane of the climb CSF, *i.e.* $0 + (1/6)[1\bar{1}00] = (1/6)[11\bar{2}0] \equiv (1/6)[1\bar{1}0]$. Thus, the phase difference will be $(2\pi/6)(h-k)$.

In a similar way, the phase differences in going from A_0^{IV} to C_0^{II} and C_0^{III} can be shown to be $(2\pi/6)(-2h-k)$ and $(2\pi/6)(h+2k)$, respectively. In each case, we denote the probability of occurrence of a climb CSF by α and thus the probability for absence of a climb CSF is $(1-3\alpha)$.

Taking the above facts into account, probability trees have been constructed as shown in Figs. 5 and 6 for a few cases. We can now write difference equations for J_m by the procedure discussed for shear CSFs.

$$J^1_{m+1} = \left[(1-3\alpha)\exp\frac{2\pi i}{3}(h-k)\right]J^0_m + \left[\alpha\exp\frac{2\pi i}{6}(h-k) + \alpha\exp\frac{2\pi i}{6}(-2h-k) + \alpha\exp\frac{2\pi i}{6}(h+2k)\right]J^1_m \quad (26)$$

$$J^0_m = \left[(1-3\alpha)\exp\frac{2\pi i}{3}(-h+k)\right]J^1_{m-1} + \left[\alpha\exp\frac{2\pi i}{6}(-h+k) + \alpha\exp\frac{2\pi i}{6}(2h+k) + \alpha\exp\frac{2\pi i}{6}(-h-2k)\right]J^0_m. \quad (27)$$

Introducing ε and η from equation (8), we have

$$J^1_{m+1} = (1-3\alpha)\varepsilon^2 J^0_m + \alpha\varepsilon\eta J^1_m \quad (28)$$

$$J^0_m = (1-3\alpha)\varepsilon^{*2} J^1_{m-1} + \alpha\varepsilon^*\eta J^0_{m-1}. \quad (29)$$

Solving (28) for J^0_{m-1}, we have

$$J^0_m = \frac{J^1_{m+1} - \alpha\varepsilon\eta J^1_m}{(1-3\alpha)\varepsilon^2}. \quad (30)$$

Substituting from (30) for J^0_m and J^0_{m-1} in (29) and simplifying, we get

$$J^1_{m+1} = \alpha(\varepsilon+\varepsilon^*)\eta J^1_m + [(1-3\alpha)^2 - \alpha^2\eta^2]J^1_{m-1}, \quad (31)$$

which is the characteristic equation. Substituting from (12) and solving for ρ yields

$$\rho = \alpha\eta\cos\frac{2\pi}{6}(h-k) \pm \left[(1-3\alpha)^2 - \alpha^2\eta^2\sin^2\frac{2\pi}{6}(h-k)\right]^{1/2}. \quad (32)$$

We denote the roots with the positive and negative signs of the discriminant respectively by Z_0 and $-Z_1$. Consideration of different possible values of h and k shows that the values of Z_0 and Z_1 reduce to the following set.

(a) h and k even (fundamental reflections):

(i) $h - k = 3N$:

$$Z_0 = 1; \quad Z_1 = 1 - 6\alpha. \quad (33)$$

(ii) $h - k = 3N \pm 1$:

$$Z_0 = -\frac{3\alpha}{2} + (1 - 6\alpha + 9\alpha^2/4)^{1/2}$$
$$Z_1 = \frac{3\alpha}{2} + (1 - 6\alpha + 9\alpha^2/4)^{1/2}. \quad (34)$$

(b) h or k odd (superlattice reflections):

(i) $h - k = 3N$:

$$Z_0 = 1 - 4\alpha; \quad Z_1 = 1 - 2\alpha. \quad (35)$$

(ii) $h - k = 3N \pm 1$:

$$Z_0 = \frac{\alpha}{2} + (1 - 6\alpha + 33\alpha^2/4)^{1/2}$$
$$Z_1 = -\frac{\alpha}{2} + (1 - 6\alpha + 33\alpha^2/4)^{1/2}. \quad (36)$$

The initial conditions can be found from the probability trees given earlier (Figs. 5 and 6).

$$J_0 = 1 \quad (37)$$

$$J_1 = \tfrac{1}{2}[(1-3\alpha)(\varepsilon^2 + \varepsilon^{*2}) + \alpha\eta(\varepsilon + \varepsilon^*)]. \quad (38)$$

Substituting the values of J_0, J_1, Z_0 and Z_1 found above, we can obtain C_0 and C_1 for different values of h and k. These are given below.

(a) h and k even (fundamental reflections):

(i) $h - k = 3N$:

$$C_0 = 1; \quad C_1 = 0. \quad (39)$$

(ii) $h - k = 3N \pm 1$:

$$C_0 = \frac{(4 - 24\alpha + 9\alpha^2)^{1/2} - (1-3\alpha)}{2(4 - 24\alpha + 9\alpha^2)^{1/2}}$$
$$C_1 = \frac{(4 - 24\alpha + 9\alpha^2)^{1/2} + (1-3\alpha)}{2(4 - 24\alpha + 9\alpha^2)^{1/2}}. \quad (40)$$

(b) h or k odd (superlattice reflections):

(i) $h - k = 3N$:

$$C_0 = 1; \quad C_1 = 0. \quad (41)$$

(ii) $h - k = 3N \pm 1$:

$$C_0 = \frac{(4 - 24\alpha + 33\alpha^2)^{1/2} - (1-3\alpha)}{2(4 - 24\alpha + 33\alpha^2)^{1/2}}$$
$$C_1 = \frac{(4 - 24\alpha + 33\alpha^2)^{1/2} + (1-3\alpha)}{2(4 - 24\alpha + 33\alpha^2)^{1/2}}. \quad (42)$$

7. Diffraction effects from CSFs on basal planes

We have shown that, for both types of CSF, J_m can be expressed in the form of (18) with different values for C_0, C_1, Z_0 and Z_1 for shear and climb CSFs. On substitution of J_m in the intensity expression [equation (2)], and performing the summations of the geometric series, we can write

$$I(h_3)/N\psi^2 = C_0\frac{1 - Z_0^2}{1 - 2Z_0\cos\pi h_3 + Z_0^2} + C_1\frac{1 - Z_1^2}{1 + 2Z_1\cos\pi h_3 + Z_1^2}. \quad (43)$$

The denominators in the two terms in the above equation have minimum values for $h_3 = l$ being even and odd integers,

respectively, and thus these terms give rise to corresponding peaks for both types of CSF.

The intensity for a shear CSF probability of 0.05 is plotted against h_3 using (43) in Figs. 7, 8 and 9. Owing to the presence of shear CSFs, the profiles are generally broadened. Fundamental reflections with $h - k = 3N$ are not affected while those with $h - k = 3N \pm 1$ show appreciable but equal broadening for even and odd values of l as illustrated in Fig. 7. Superlattice reflections with $h - k = 3N$ and l even also show considerable broadening. As is apparent from Fig. 9, superlattice reflections with $h - k = 3N \pm 1$ show appreciable but equal broadening for even and odd values of l. Further, superlattice reflections with $h - k = 3N \pm 1$ show a smaller broadening than that for reflections with $h - k = 3N$, as is clear from Figs. 8 and 9.

The intensity for a climb CSF probability of 0.05 is plotted as a function of h_3 for fundamental and superlattice reflections in Figs. 10, 11 and 12. For fundamental reflections with $h - k = 3N \pm 1$, peaks occur at $h_3 = l$, where l is an integer as shown in Fig. 10. Reflections with l even are considerably broader than those with l odd. For superlattice reflections with $h - k = 3N$ (Fig. 11), a broad peak occurs for $h_3 = l$ with l being an even integer. On the other hand, for superlattice reflections with $h - k = 3N \pm 1$ (Fig. 12), broadened peaks occur at $h_3 = l$ where l is an integer. The broadening of reflections with l odd is somewhat greater than that for those with l even. Quantitative aspects of broadening are discussed in the following section.

7.1. Integrated Intensity

The total energy of the diffracted beam can be measured and is known as the integrated intensity. In electron diffraction, double diffraction and dynamical effects are usually present and as such the above kinematic treatment is not applicable as far as integrated intensities are concerned (Cowley, 1981). We, therefore, restrict our calculation of the integrated intensity for powder diffraction profiles.

An analytical expression for the integrated intensity, T, of a reflection can be obtained by integrating the intensity over one full period of the reflection. Corresponding to each of the two maxima in $I(h_3)$, we have

$$T_j = \int_0^2 \left[C_j \frac{1 - Z_j^2}{1 - 2Z_j(-1)^j \cos \pi h_3 + Z_j^2} \right] \mathrm{d}h_3 = 2C_j \qquad \text{for } j = 0 \text{ or } 1. \quad (44)$$

The values of C_0 and C_1 for shear as well as climb CSFs have been given earlier. Utilizing these, one can evaluate the changes in the integrated intensities owing to the presence of shear and climb CSFs. The fractional changes in integrated intensities owing to the simultaneous presence of shear and climb CSFs for small values of the probabilities (respectively α_s and α_c) of their occurrence can be found by assuming that the effects are additive and are given below.

(a) h and k even (fundamental reflections):

(i) $h - k = 3N$:

$$\Delta T_0/T_0 = 0; \quad \Delta T_1/T_1 = 0. \quad (45)$$

(ii) $h - k = 3N \pm 1$:

$$\Delta T_0/T_0 = -(9/2)\alpha_s; \quad \Delta T_1/T_1 = +(3/2)\alpha_s. \quad (46)$$

(b) h or k odd (superlattice reflections):

(i) $h - k = 3N$:

$$\Delta T_0/T_0 = 0; \quad \Delta T_1/T_1 = 0. \quad (47)$$

(ii) $h - k = 3N \pm 1$:

$$\Delta T_0/T_0 = +(3/2)\alpha_s; \quad \Delta T_1/T_1 = -(1/2)\alpha_s. \quad (48)$$

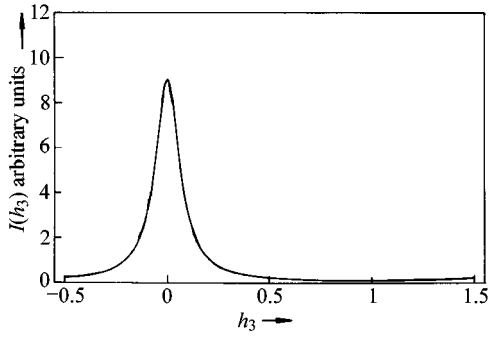

Figure 8
The diffracted intensity for superlattice reflections with $h - k = 3N$ for $\alpha_s = 0.05$.

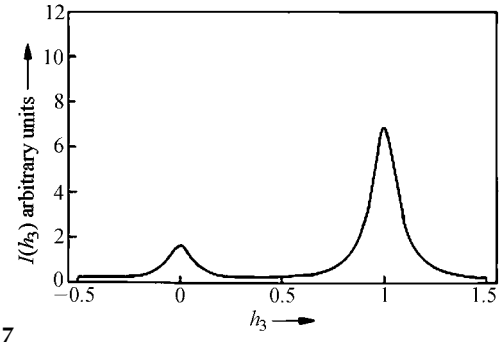

Figure 7
The diffracted intensity for fundamental reflections with $h - k = 3N \pm 1$ for $\alpha_s = 0.05$.

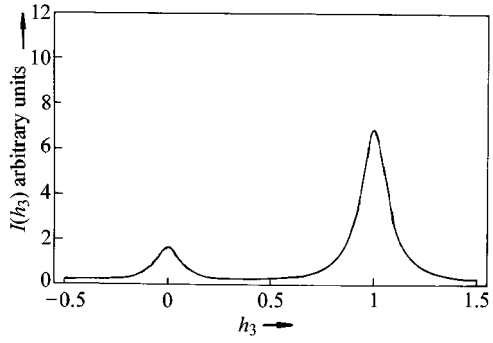

Figure 9
The diffracted intensity for superlattice reflections with $h - k = 3N \pm 1$ for $\alpha_s = 0.05$.

The integrated intensities of reflections with $h - k = 3N$ remain unchanged while those for reflections with $h - k = 3N \pm 1$ are affected by the presence of shear as well as climb CSFs. However, the effects of the latter vanish for small values of α_c.

7.2. Integral breadth

Using the definition of integral breadth (β) as the ratio of the integrated intensity and the profile maximum, we can write in general

$$\beta_j = 2\frac{1 - Z_j}{1 + Z_j} \quad \text{for } j = 0 \text{ or } 1. \tag{49}$$

The values of Z_0 and Z_1 for shear as well as climb CSFs have been given earlier and yield the following expressions for small values of the probabilities of occurrence of shear and climb CSFs.

(a) h and k even (fundamental reflections):

(i) $h - k = 3N$:

$$\beta_o = 0. \tag{50}$$

(ii) $h - k = 3N \pm 1$:

$$\beta_o = \tfrac{9}{2}(\alpha_s + \alpha_c), \quad \beta_1 = \tfrac{3}{2}(3\alpha_s + \alpha_c). \tag{51}$$

(b) h or k odd (superlattice reflections):

(i) $h - k = 3N$:

$$\beta_o = 4(\alpha_s + \alpha_c). \tag{52}$$

(ii) $h - k = 3N \pm 1$:

$$\beta_o = \tfrac{5}{2}(\alpha_s + \alpha_c), \quad \beta_1 = \tfrac{1}{2}(5\alpha_s + 7\alpha_c). \tag{53}$$

The above expressions are for the integral breadth as a function of h_3 in reciprocal space. However, we experimentally measure integral breadth in terms of 2θ in degrees in a powder pattern. The necessary diffraction geometry for obtaining the relation between these quantities has been considered earlier (Ghosal *et al.*, 2003). The relation between the breadth in reciprocal space (β) and the corresponding one in real space [$\beta(2\theta)^\circ$] is

$$\beta(2\theta)^\circ = \left[\frac{360}{\pi}|l|\left(\frac{d}{c}\right)^2 \tan\theta\right]\beta. \tag{54}$$

8. Discussion

Prasad (1975) has earlier considered the diffraction effects of shear CSFs on basal planes in a $D0_{19}$ structure. To compare his results with ours, it is convenient to start with his characteristic equation [equation (8)].

$$\rho^4 - 2\rho^2[\alpha_1^2 + (1 - \alpha_1)^2] + (1 - 4\alpha_1 + 6\alpha_1^2) - 2\alpha_1^2 \cos\frac{2\pi}{6}(h - k) = 0, \tag{55}$$

where α_1 is the probability of occurrence of CSFs with shift vector $1/6[1\bar{1}00]$. Some of the higher-order terms in α_1 have been neglected by Prasad in writing the above equation. The complete equation is

$$\rho^4 - 2\rho^2[\alpha_1^2 + (1 - \alpha_1)^2] + [\alpha_1^4 - (1 - \alpha_1)^4] - 2\alpha_1^2(1 - \alpha_1)^2 \cos\frac{2\pi}{3}(h - k) = 0. \tag{56}$$

It can be shown that the expression on the left-hand side can be factorized. Only one of the two factors is physically relevant and is given below:

$$\rho^2 - [\alpha_1^2 + (1 - \alpha_1)^2] - 2\alpha_1(1 - \alpha_1)\cos\frac{2\pi}{6}(h - k) = 0. \tag{57}$$

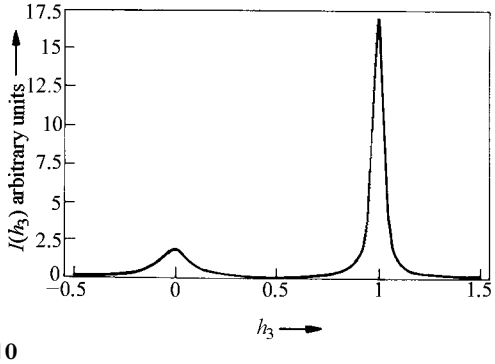

Figure 10
The diffracted intensity for fundamental reflections with $h - k = 3N \pm 1$ for $\alpha_c = 0.05$.

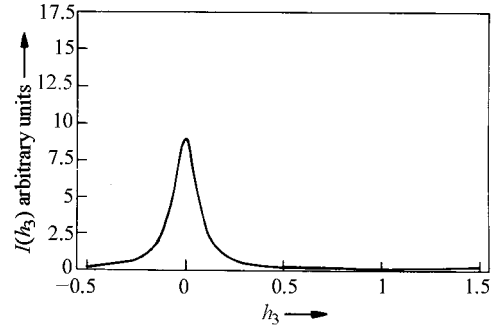

Figure 11
The diffracted intensity for superlattice reflections with $h - k = 3N$ for $\alpha_c = 0.05$.

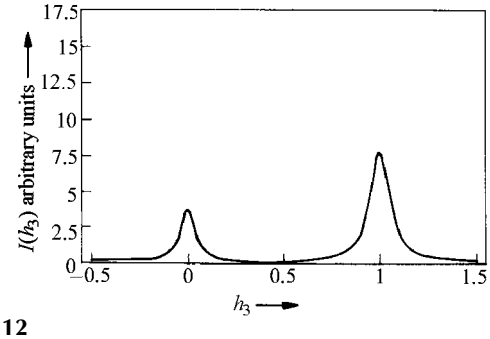

Figure 12
The diffracted intensity for superlattice reflections with $h - k = 3N \pm 1$ for $\alpha_c = 0.05$.

Table 1
Diffraction effects of CSFs in $D0_{19}$ structures.

			Diffraction effects			
			Fundamental reflections		Superlattice reflections	
Plane	Shift vector	Fault	$h-k=3N$	$h-k=3N\pm1$	$h-k=3N$	$h-k=3N\pm1$
(0001)	$1/6\langle\bar{1}100\rangle$	Shear CSF	(i) Integrated intensity unaffected	(i) Integrated intensity affected; fractional change (for $\alpha \ll 1$) is $-9\alpha/2$ for l even and $+3\alpha/2$ for l odd.	(i) Integrated intensity unaffected	(i) Integrated intensity affected; fractional change (for $\alpha \ll 1$) is $+3\alpha/2$ for l even and $-\alpha/2$ for l odd.
			(ii) No peak broadening	(ii) Integral breadth is proportional to $9\alpha/2$ (for $\alpha \ll 1$)	(ii) Integral breadth (for $\alpha \ll 1$) is proportional to 4α	(ii) Integral breadth (for $\alpha \ll 1$) is proportional to $5\alpha/2$.
			(iii) No peak asymmetry	(iii) No peak asymmetry	(iii) No peak asymmetry	(iii) No peak asymmetry
(0001)	$1/6\langle\bar{1}10\bar{3}\rangle$	Climb CSF	(i) Integrated intensity unaffected	(i) Integrated intensity affected; no effects to first order	(i) Integrated intensity unaffected	(i) Integrated intensity affected; No effects to first order
			(ii) No peak broadening	(ii) Integral breadth (for $\alpha \ll 1$) is proportional to $9\alpha/2$ for l even and $3\alpha/2$ for l odd	(ii) Integral breadth (for $\alpha \ll 1$) is proportional to 4α	(ii) Integral breadth (for $\alpha \ll 1$) is proportional to $5\alpha/2$ for l even and $7\alpha/2$ for l odd.
			(iii) No peak asymmetry	(iii) No peak asymmetry	(iii) No peak asymmetry	(iii) No peak asymmetry

Simultaneous consideration of other types of shear CSF's with probabilities α_2 and α_3 {shift vectors $(1/6)[\bar{1}010]$ and $(1/6)[01\bar{1}0]$, respectively} leads to the following generalized characteristic equation:

$$\rho^2 - [\alpha_1 + (-1)^h\alpha_2 + (-1)^k\alpha_3]^2 - (1-\alpha_1-\alpha_2-\alpha_3)^2 - 2[\alpha_1 + (-1)^h\alpha_2 + (-1)^k\alpha_3](1-\alpha_1-\alpha_2-\alpha_3) \times \cos\frac{2\pi}{6}(h-k) = 0. \quad (58)$$

It is easy to see that the above equation reduces to equation (57) when $\alpha_1 \neq 0 = \alpha_2 = \alpha_3$ and to equation (13) when $\alpha_1 = \alpha_2 = \alpha_3 = \alpha \neq 0$. Thus, there is no basic discrepancy between his formulation and ours. We believe that the situation considered by us is physically more realistic. Such CSFs are expected to arise during deformation. For polycrystalline samples, the applied stresses will be oriented randomly and, thus, there is no reason to expect the differential formation of the three types of CSF.

Further, Prasad does not carry out his analysis to a point where directly usable results are obtained. For example, there is no mention of the distinction between the effects for fundamental and superlattice reflections and the conditions on h and k mentioned are incomplete in several cases.

We mention some of the salient features of the results by consideration of the more general equation (58). The diffraction effects for fundamental reflections are identical to those discussed above except that α should be interpreted as an average of α_1, α_2 and α_3. This can be clearly seen by letting h and k be even numbers in equation (58) and comparing with equation (13).

Superlattice reflections (h or k odd) require more detailed consideration. We have to consider three possibilities, namely (i) h and k odd, (ii) h odd and k even, (iii) h even and k odd. For the first case, equation (58) has the solutions

$$\rho = \pm(1-2\alpha_2-2\alpha_3) \quad \text{for } h-k=3N$$
$$\rho = \pm\left(1-\frac{3\alpha_1+\alpha_2+\alpha_3}{2}\right) \quad \text{for } h-k=3N\pm1,$$

yielding the following integral breadths for reflections with h and k odd:

$$\beta = 2(\alpha_2+\alpha_3) \quad \text{for } h-k=3N$$
$$\beta = (3\alpha_1+\alpha_2+\alpha_3)/2 \quad \text{for } h-k=3N\pm1.$$

Similarly, for reflections with h odd and k even, we have

$$\beta = 2(\alpha_3+\alpha_1) \quad \text{for } h-k=3N$$
$$\beta = (\alpha_1+3\alpha_2+\alpha_3)/2 \quad \text{for } h-k=3N\pm1$$

and finally, for those with h even and k odd, we obtain

$$\beta = 2(\alpha_1+\alpha_2) \quad \text{for } h-k=3N$$
$$\beta = (\alpha_1+\alpha_2+3\alpha_3)/2 \quad \text{for } h-k=3N\pm1.$$

It is interesting to note that these expressions become identical for $\alpha_1 = \alpha_2 = \alpha_3 = \alpha$ (treated by us) but are distinct for cases such as those with $\alpha_1 \neq 0 = \alpha_2 = \alpha_3$ (considered by Prasad). However, for reflections in powder patterns, a given reflection has several components and one observes an average broadening. Since an equal number of components corresponding to each of the above cases are present in any powder reflection, we have

$$\beta = 4(\alpha_1+\alpha_2+\alpha_3)/3 \quad \text{for } h-k=3N$$
$$\beta = 5(\alpha_1+\alpha_2+\alpha_3)/6 \quad \text{for } h-k=3N\pm1.$$

Thus, the distinction mentioned above is lost for powder reflections and the only observable quantity is $(\alpha_1+\alpha_2+\alpha_3) = 3\bar{\alpha}$.

The diffracted intensity as given by equation (43) for $\alpha = 0.05$ is plotted as a function of h_3 in Figs. 7 to 12. The fundamental reflections with $h-k=3N$ are unaffected by shear or climb CSFs on basal planes and exhibit delta peaks in re-

ciprocal space. Hence, these are not illustrated. Further, the integrated intensity of superlattice reflections with $h - k = 3N$ is unchanged [equation (47) and Figs. 8 and 10]. On the other hand, for reflections with $h - k = 3N \pm 1$ and l even, the integrated intensity of fundamental reflections decreases sharply while that of superlattice reflections increases somewhat, the change being linearly proportional to the shear fault probability. A similar but opposite effect occurs for the case of $h - k = 3N \pm 1$ and l odd reflections. Climb CSFs do not affect the integrated intensity to first order in the fault probability.

As regards profile broadening, fundamental reflections with $h - k = 3N$ are not broadened while the broadening is proportional to $(9\alpha_s + 9\alpha_c)$ and $(9\alpha_s + 3\alpha_c)$ for those with $h - k = 3N \pm 1$ and l even and odd, respectively. For superlattice reflections with $h - k = 3N$, the broadening is proportional to $(8\alpha_s + 8\alpha_c)$ and for those with $h - k = 3N \pm 1$ and l even and odd, respectively, it is proportional to $(5\alpha_s + 5\alpha_c)$ and $(5\alpha_s + 7\alpha_c)$. For fundamental reflections, the integral breadths are not affected by pure APBs and thus we should expect shear and climb CSFs to exhibit effects similar to those of deformation and growth faults in a disordered c.p.h. structure. Christian (1954) and Wilson (1942) have formulated the theory of diffraction for these situations. A comparison with their results shows that the change in integrated intensity and the broadening in the two cases are identical if Christian's deformation fault probability or Wilson's growth fault probability is identified to be equal to our 3α.

Measurements of changes of integrated intensities of fundamental or superlattice reflections with $h - k = 3N \pm 1$ can directly yield a value for α_s. However, the accuracy of these measurements is generally not sufficiently high for satisfactory evaluation of α_s. Measurements of integral breadths of fundamental reflections with $h - k = 3N \pm 1$ and l even or superlattice reflections with l even yield an estimate of $(\alpha_s + \alpha_c)$. Similarly, fundamental and superlattice reflections with $h - k = 3N \pm 1$ and l odd yield estimates for $(3\alpha_s + \alpha_c)$ and $(5\alpha_s + 7\alpha_c)$, respectively. Combining the second estimate with either the first or third estimates can lead to sufficiently accurate independent estimates of α_s and α_c.

Shear or climb CSFs do not cause any asymmetry in the reflections in reciprocal space. However, as pointed out by Guinier (1963), reflections of the type $kh0$ show a profile asymmetry in 2θ space when they are broadened along h_3 in reciprocal space. This is purely due to geometrical effects and the asymmetry is confined only to real space (2θ space), and thus should not be confused with the asymmetry in reciprocal space due to any other fault while analysing the diffraction effects. This geometrical profile asymmetry due to line broadening is negligible for reflections other than $kh0$.

9. Conclusions

The diffraction effects of shear and climb CSFs lying on basal planes of a $D0_{19}$ structure are summarized in Table 1. The shear and climb CSF probabilities can be evaluated by measuring the profile broadening (and the integrated intensity) for a suitable set of reflections. This can in turn be used to calculate the CSF energy, which is an important property governing the deformation behaviour of the material. However, the diffraction effects due to the possible presence of other faults or APBs lying on basal as well as non-basal planes need also be considered in order to understand and correlate the observed effects properly.

The authors thank the Department of Science & Technology, Government of India, New Delhi, for financial help to carry out the work through a Research Project and one of the authors (PG) is grateful to Director, DMRL, for his kind encouragement and permission to publish this work.

References

Christian, J. W. (1954). *Acta Cryst.* **7**, 415–416.
Cowley, J. M. (1981). *Diffraction Physics.* Amsterdam: North-Holland.
Ghosal, P. (1996). PhD thesis, Banaras Hindu University, Varanasi, India.
Ghosal, P., Ramachandra, C. & Lele, S. (1993). *Scr. Metall. Mater.* **28**, 477–482.
Ghosal, P., Ramachandra, C. & Lele, S. (2003). *Philos. Mag.* A. Submitted.
Guinier, A. (1963). *X-ray Diffraction in Crystals, Imperfect Crystals and Amorphous Bodies*, pp. 185–220. San Francisco: W. H. Freeman.
Mikkola, D. E. & Cohen, J. B. (1965). *Local Atomic Arrangements as Studied by X-rays*, edited by J. B. Cohen & J. E. Hilliard, pp. 289–340. New York: Gordon and Breach.
Mikkola, D. E. & Cohen, J. B. (1966). *Acta Metal.* **14**, 105–122.
Prasad, B. (1975). *Acta Cryst.* A**31**, 240–245.
Prasad, B. & Lele, S. (1971). *Acta Cryst.* A**27**, 54–64.
Warren, B. E. (1969). *X-ray Diffraction*, pp. 277–304. Reading, MA: Addison-Wesley.
Wilson, A. J. C. (1942). *Proc. R. Soc. London Ser. A*, **180**, 277–285.
Wilson, A. J. C. (1943). *Proc. R. Soc. London Ser. A*, **181**, 360–368.
Wilson, A. J. C. & Zsoldos, L. (1966). *Proc. R. Soc. London Ser. A*, **290**, 508–514.